Coordination of DERs and Flexible Loads to Support Transmission Voltages in Emergency Conditions

Francisco Escobar, *Student Member, IEEE,* Juan M. Víquez, Jorge García, Petros Aristidou, *Senior Member, IEEE,* and Gustavo Valverde, *Senior Member, IEEE*

***Abstract*—The large-scale integration of renewable generation and the gradual decommissioning of conventional power plants has led to decreased availability of resources for providing services and support to the bulk transmission grid. This paper presents a novel methodology for providing support to the bulk transmission system through the control of thousands of small distributed energy resources (DERs), located in distribution systems. This control scheme is expected to serve jointly with other classical countermeasures against instability conditions. The proposed method is model-free, scalable, and does not rely on extensive communication infrastructure. It integrates an online method (New LIVES) to monitor the voltage stability status of the transmission system, a rule-based decentralized decision algorithm, and the local DER mechanisms implementing the control actions. The proposed approach is implemented on a combined transmission and distribution test system with over 4200 low-voltage buses and the dynamic simulation results illustrate its flexibility, practicality, and tractability.**

***Index Terms*—Ancillary services, demand response, distributed energy resources, flexible loads, transmission and distribution, TSO-DSO coordination, voltage stability.**

I. Introduction

MODERN power systems are characterized by the decommissioning of nuclear and coal-fired power stations, and the integration of renewable energy systems. Many of these generators are being installed at the distribution system level, which poses new challenges to Transmission System Operators (TSOs) who have limited, if not null, visibility and control over these units. Moreover, the conventional power plants, due to be decommissioned, currently offer several services that are essential for the secure operation of power systems [1]. This motivates the TSOs to coordinate with Distribution System Operators (DSOs) to exploit the resources available in the Distribution Networks (DNs) for ancillary services [2], [3].

The restrictions on building new transmission corridors in many countries are also recognized as a major threat for the system's voltage stability. Hence, classical countermeasures against voltage instability can be reinforced with the participation of Distributed Energy Resources (DERs).

Mechanically switched capacitors near loads are typically used to inject reactive power in response to low voltages, and the shunt reactors, used to prevent overvoltages, may be disconnected to counteract voltage instability [4], [5]. Emergency control actions of On-Load Tap Changers (OLTCs) in step-down transformers can be achieved by OLTC blocking [6], or by reducing OLTC setpoints to exploit the sensitivity of loads to voltage [7]. In addition, selective Load Shedding (LS), generally used as a last resort, is a very effective countermeasure if the action takes place before the long-term equilibrium point falls outside the region of attraction [8]. The authors in [9] even propose a robust LS scheme against long-term voltage instability that does not require communication between controllers, since they can be implicitly coordinated through network voltages.

Considerable research efforts have been devoted to controlling utility-scale DERs for the provision of external grid support. Some of these include the regulation of Transmission Network (TN) bus voltages [10], model-free optimal coordination of DERs to provide TN services [11], frequency regulation of Battery Energy Storage Systems (BESSs) [12], strategies to enhance the dynamic thermal rating of transmission lines [13], and control schemes to increase the TN voltage stability and loadability margins [14].

In [15], the authors present a control scheme where large-scale Dispersed Generators (DGs) connected at Medium Voltage (MV) level inject reactive power to support the transmission system once the so-called pilot bus reports a voltage value lower than a predefined threshold. However, as explained in [16], the monitoring of only bus voltage magnitudes may not suffice to detect, in due time, voltage instability conditions. The authors in [17] evaluate the provision of active and reactive power from large-scale DERs to support TNs in emergency conditions along with other countermeasures such as OLTC blocking, or OLTC voltage setpoint reduction. The latter are particularly effective in presence of voltage-dependent loads. In this direction, the authors in [18] proposed the synchronization of reactive power injections of large-scale DGs with transformer's OLTC actions. This coordination avoids the undesired restoration of voltage-dependent loads as the DGs inject reactive power to the TN.

New methodologies based on AC Optimal Power Flow (AC-OPF) formulations are used to estimate the flexibility of Active Distribution Networks (ADNs) at the TSO-DSO interface. The works in [19]–[21] estimate the flexibility range of active and reactive power at the TSO-DSO interface by means of capability charts of DNs to aid the operation of TNs. The impact of grid topology changes and transformer's tap position changes on the flexibility provision from ADNs is analyzed in [22], and the value of the flexibility at the TSO-DSO interface is measured in [23] by computing the DSO capability curves and the TSO desirability surfaces.

F. Escobar, J. M. Víquez, J. García, and G. Valverde are with the School of Electrical Engineering, University of Costa Rica, San José 2060, Costa Rica (email: gustavo.valverde@ucr.ac.cr).

Petros Aristidou is with the Department of Electrical Engineering, Computer Engineering & Informatics, Cyprus University of Technology, Limassol 3036, Cyprus (email: petros.aristidou@cut.ac.cy).

Large penetration levels of DERs are expected to affect the stability of bulk power systems [24], [25]. In long-term voltage instability scenarios, large-scale DGs driven by DN voltage controllers may accelerate a voltage collapse if the latter ignore the TN conditions [7]. However, they could contribute to corrective actions against voltage instability if their control logic changes after receiving an alarm signal. This concept was extended in [26], where DGs enhance the system stability while preserving the DN integrity. The latter also focuses on large-scale DERs, but it uses the local TN-bus and DN-bus voltages to define the contribution of the available resources. In [27], the provision of voltage ancillary services with DERs is designed for improving short-term voltage stability. The methodology transmits voltage measurements to DGs from Phasor Measurement Units (PMUs) at the transmission level, and takes into consideration any equipment with reactive power capabilities at the MV level. However, this approach does not consider the resources available in Low Voltage (LV) systems.

In the coming years, it is expected that aggregators will control customer-owned DERs and Flexible Loads (FLs) to provide services to DSOs and TSOs [2], [28]. The work in [29] presents an AC-OPF-based methodology to estimate the volume of services that aggregators can provide. The authors in [30] present a methodology for the coordination of residential Demand Response (DR) with the operational constraints of the local LV system. A model-free coordination of thousands of small-scale DERs is proposed in [31] to control the reactive power exchange at the TSO-DSO interface in steady-state conditions. A centralized AC-OPF with the participation of small-scale DERs is proposed in [32] to provide steady-state voltage support to the TN, while optimizing the DN operation and satisfying the power quality constraints. The authors in [33] present an AC-OPF-based formulation where small-scale BESSs at LV systems may provide frequency regulation services.

The literature has scarcely reported on long-term voltage stability enhancement with the resources installed at LV levels [34]. The use of small-scale DERs to support TNs in emergency situations poses additional challenges in terms of communication, coordination, availability, and response of hundreds or thousands of agents.

In this work, a new coordination scheme of DERs and FLs is presented to prevent voltage collapses. The proposed coordinator sends periodic signals to the downstream devices according to the TN condition, which is monitored by PMUs. However, the former has no knowledge about the actual condition and individual response of each resource. The DERs and FLs decide how to respond based on local measurements only. It is assumed that they are committed with the coordinator (as an aggregator) to provide these services. The way how these services may be compensated is beyond the scope of this paper.

Compared to previous works that consider DERs to support TN bus voltages, e.g. [7], [26], [35], this new scheme includes the participation of small-scale DERs installed at LV systems. Moreover, these units can respond and support during emergency situations, a step forward from recent schemes designed to operate under normal TN conditions [11], [31], [32]. Since the coordinator does not receive information from DERs or make use of a network model, it is scalable to large systems. The contributions of this paper are:

- A novel model-free control scheme that is highly scalable to coordinate thousands of small-scale devices to support the actions of the TSO. The coordinator and the dispersed resources only use real-time measurements to act during the long-term voltage instability scenarios.
- A practical logic for the coordinator to issue control signals based on the evolution of the load conductance and the active power at the boundary buses of a weak area, computed with synchrophasors.
- Design of local controllers that enable DERs and FLs to interpret and respond to the signals issued by the coordinator.

The proposed scheme is essentially a temporary support rather than permanent, limited by the time-dependent availability and penetration level of DER units and FLs. Therefore, it is intended to complement the more classical, and consistently effective, countermeasures to maintain system stability, e.g. start-up of fast units located near the load centers, emergency control of OLTCs, and undervoltage LS.

This scheme does not deteriorate the DN integrity and respects the capability of the DERs and FLs, as they decide how to respond based on local measurements. Detailed models of these units are used in a Transmission-Distribution (T-D) co-simulation platform to validate the effectiveness of the proposed coordination.

The remainder of this paper is organized as follows: The coordination scheme is presented in Section II. The local control actions carried out by DERs and FLs are presented in Section III. Finally, simulation results and conclusions are presented in Sections IV and V, respectively.

II. Proposed Coordination Scheme

The coordination of DERs and FLs is carried out at step-down substations where the DN can provide active and reactive power support. To ensure that the DN has enough flexibility, the methodologies from [19]–[21], [23], [36] can be employed. There might be as many coordinators as TN load buses, and they are independent from each other. Coordination between substations, which could lead to a better management of voltage instability, is beyond the scope of this paper.

A. Principles

The coordinators send signals to the corresponding DERs and FLs to change their power output, so that the net power demand at the step-down substation favors the TN in emergency conditions. These signals are chosen based on information taken at the High Voltage (HV) level alone, as depicted in Fig. 1.

The DERs and FLs may include utility-scale and small-scale units located at the MV and LV networks, respectively. Moreover, one-way communication is used, and it takes place through a common signal Σ that is broadcast to all the downstream units. The latter receive the signal and decide whether or not to participate based on their local conditions and on the level of emergency issued. These decisions are taken locally without knowledge of the overall system performance.

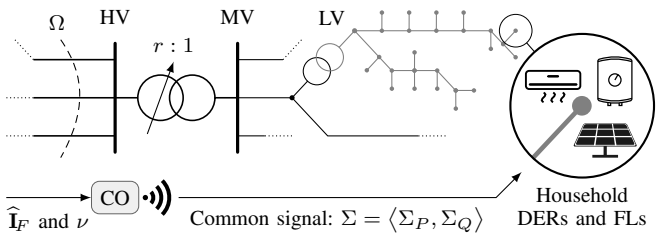

Fig. 1. Control scheme with a coordinator (CO) and one-way communication.

The control loop is closed by measurements processed by each coordinator, which should reflect the response of the DERs and FLs. These include PMU measurements of voltage and currents entering at boundary buses, and a vector with the field winding current measurements $\widehat{\mathbf{I}}_F$ of large synchronous generators connected to the TN. In cases where power plants cannot send the measurements contained in $\widehat{\mathbf{I}}_F$ in real time, it would suffice that they report the status of their field current: below limit, over limit, or limited. The way how these measurements are processed to choose the value of Σ is further explained in Sections II-B and II-C. In addition, each coordinator has a binary input signal ν to either start requesting support or cease it when no longer needed.

Given the one-way communication, along with the heterogeneity and the large number of DERs and FLs, the coordinator has no direct knowledge of their status, internal states, or availability to provide services.

The signal Σ has two channels that allow independent requests of active (P) and reactive (Q) power, and they are written as $\Sigma = \langle \Sigma_P, \Sigma_Q \rangle$ in the remainder of the paper. The numerical value that is broadcast through each channel relates to the degree of participation required by the coordinator. It means that the units will react more aggressively to larger values of Σ_P and Σ_Q. These values need not be updated continuously, since the proposed coordination scheme addresses long-term stability [37]. Instead, they can be updated intermittently with a sampling period τ_s that is in the order of a few seconds. Larger values of τ_s are not recommended, as several instability-inducing disturbances, such as OLTC and Overexcitation Limiter (OEL) actions, could take place between consecutive coordinator commands.

The precise form of Σ can be formalized by interpreting it as a discrete-time function of the form $\Sigma\colon \mathcal{T} \to \mathcal{S} \times \mathcal{S}$, where $\mathcal{T} = \{t_k = k\tau_s \mid k \in \mathbb{N}\}$ is the set of time samples and $\mathcal{S} = \{1, \ldots, N\}$ is the set of possible values for Σ_P and Σ_Q. In this paper, $N = 5$ so that Σ remains in $\langle 1, 1 \rangle$ under normal conditions, and it can take higher values up to $\langle 5, 5 \rangle$ after severe disturbances. However, finer requests could be sent by reducing τ_s and increasing N. Furthermore, negative integers could be included in $\mathcal{S}$ to request the DERs and FLs to demand more active or reactive power. However, increasing the FL demand is counterproductive to attack voltage instability.

This new coordination scheme is highly scalable and can be readily implemented using existing technology, one example being Advanced Metering Infrastructure (AMI). The problem of communicating with dissimilar DERs and FLs, each having its own internal controllers and possibly communicating through vendor-specific protocols, can be solved by leveraging home-automation systems. Inside each building, an entity would keep track of Σ and then translate these requests into parameters that each controllable device in the building can understand. Section III presents the way how each device responds to the coordinator signals.

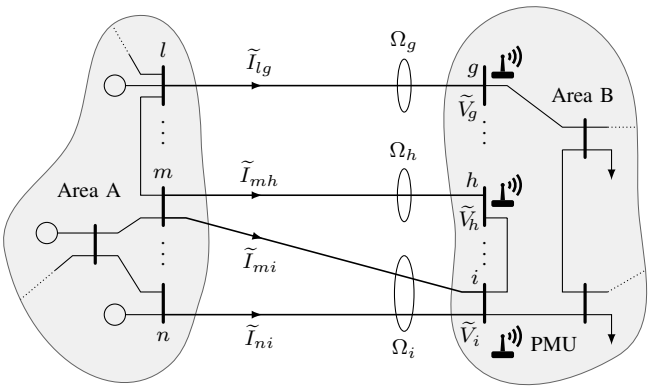

Fig. 2. Location of PMUs to compute the NLI at boundary buses of the weak area B.

B. Detection of Voltage Emergency Conditions

Voltage instability results from the inability of the combined generation and transmission system to supply the power requested by the loads [8]. This condition can be detected in real-time to take remedial actions and prevent blackouts [38], [39].

In this work, each coordinator detects instability conditions based on the New LIVES indicator (NLI), introduced in [16]. Essentially, this indicator measures the ratio of the change of power transmitted to a load to the change of load conductance, which relates in turn to the load's demand. This is a generalization of the Local Identification of Voltage Emergency Situations (LIVES) method [40] and has the advantage that secondary voltages and tap ratios need not be monitored directly. The NLI usually takes values between 0.5 and 1.5 during normal operation, and then it drops to negative values when instability is detected. Calculations performed on real historic measurements show that the NLI is effective, selective, and reliable [41]. The calculation procedure is explained below.

Consider a weak area B that is fed through a transmission corridor (cut-set), as depicted in Fig. 2. PMUs are installed at the boundary TN buses in area B to measure the incoming currents $\widetilde{I}$ and the bus voltages $\widetilde{V}$. Note that the total imported current at bus i from all the lines crossing Ω_i is

$$\widetilde{I}_i = -\sum_{\omega \,\in\, \Omega_i} \widetilde{I}_{i\omega}\,. \tag{1}$$

The active power transferred to bus i and the load conductance in this bus are computed from

$$P_i = \mathrm{Re}\left(\widetilde{V}_i \widetilde{I}_i^*\right), \tag{2}$$

$$G_i = \mathrm{Re}\left(\widetilde{I}_i / \widetilde{V}_i\right). \tag{3}$$

The PMU measurements of voltage and currents are collected at a high sampling rate to compute P_i and G_i every $\Delta t =$

$20\,\mathrm{ms}$. Moreover, a moving average with M samples is used to compute the values $\overline{G}_i$ and $\overline{P}_i$ at time t_k:

$$\overline{G}_i(t_k) = \frac{1}{M}\sum_{j=0}^{M-1} G_i(t_k - j\Delta t)\,, \tag{4}$$

$$\overline{P}_i(t_k) = \frac{1}{M}\sum_{j=0}^{M-1} P_i(t_k - j\Delta t)\,. \tag{5}$$

The changes in transferred power and load conductance are computed based on a time difference ΔT of several seconds, e.g. $7\,\mathrm{s}$. In the case of the conductance, this change is

$$\Delta G_i(t_k) = \overline{G}_i(t_k) - \overline{G}_i(t_k - \Delta T)\,, \tag{6}$$

and similarly for $\Delta P_i(t_k)$. To minimize noise, these changes are recorded as long as

$$\Delta G_i(t_k)/\overline{G}_i(t_k - \Delta T) \geq \varepsilon \tag{7}$$

for a predefined threshold ε. In practice, this threshold would be set based on historic measurements so that no changes are recorded under normal conditions. An additional filtering is provided by taking an M_d-sample moving average $\overline{\Delta G}_i$ at t_k:

$$\overline{\Delta G}_i(t_k) = \frac{1}{M_d}\sum_{j=0}^{M_d-1} \Delta G_i(t_{k-j})\,, \tag{8}$$

and similarly for $\overline{\Delta P}_i(t_k)$. The NLI of bus i at time t_k is then

$$\mathrm{NLI}_k = \frac{\overline{\Delta P}_i(t_k)}{\overline{\Delta G}_i(t_k)}\,. \tag{9}$$

To further smoothen NLI_k, a final filtering is applied by taking a 10-sample moving average, which results in $\overline{\mathrm{NLI}}_k$.

Minor modifications from the original NLI in [16] were made, given that the indicator is part of the proposed coordinator's control loop. Firstly, when (7) is not met at t_k, the value of $\overline{\mathrm{NLI}}_k$ is set to $\overline{\mathrm{NLI}}_{k-1}$. Secondly, a reset of $\overline{\Delta G}_i(t_k)$, $\overline{\Delta P}_i(t_k)$, and $\overline{\mathrm{NLI}}_k$ is carried out if $\overline{\mathrm{NLI}}_k$ remains constant at a negative value, for instance with 25 consecutive samples, and no field current of any generator exceeds its maximum allowed value.

A reset of $\overline{\Delta G}_i(t_k)$ implies that the M_d samples of ΔG_i in (8) are discarded. After the reset, (8) is computed with the new available samples of ΔG_i, without having to wait for M_d samples. The same logic applies to $\overline{\Delta P}_i(t_k)$ and $\overline{\mathrm{NLI}}_k$.

Each coordinator must be governed by the $\overline{\mathrm{NLI}}$ of a single boundary bus. This association can be defined offline by simulating critical contingencies followed by a load reduction at the bus where the coordinator is placed. The coordinator would then respond to the $\overline{\mathrm{NLI}}$ whose load reduction helps the most, either delaying its zero-crossing or preventing it altogether. The coordinators are thus independent, and do not necessarily monitor the same boundary bus.

C. Support Requests

Each coordinator follows the binary decision tree of Fig. 3 to select the values of Σ. When the coordinator is active, i.e. $\nu = 1$, it takes decisions based on the $\overline{\mathrm{NLI}}$ of the corresponding boundary bus, and the remote measurements $\widehat{\mathbf{I}}_F$.

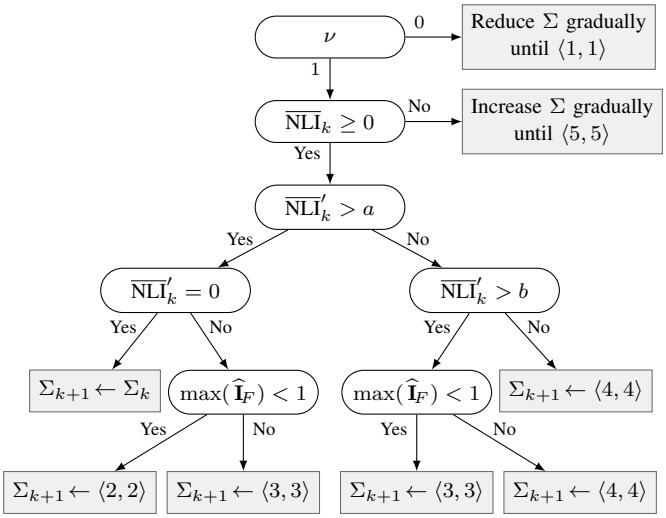

Fig. 3. Proposed binary decision tree for requesting DER and FL actions.

After traversing the tree at t_k, it selects the value Σ_{k+1} to be broadcast at t_{k+1}.

$\widehat{\mathbf{I}}_F$ is used to foresee the activation of one or several OELs, which is a sign of weakness in the system, but not of instability. Each measurement in the vector $\widehat{\mathbf{I}}_F$ is normalized so that its value is 1 if the field current equals the thermal limit of the corresponding winding. These measurements are updated every time that the decision tree is traversed, i.e. every τ_s seconds.

From the decision tree in Fig. 3, if $\overline{\mathrm{NLI}}_k < 0$, an emergency situation has been detected, and all the available resources should be deployed. To prevent the agents from synchronizing, and to leave time for the evolution of the situation without exhausting the participation of DERs and FLs, both Σ_P and Σ_Q are increased gradually. Assuming that the first negative value of $\overline{\mathrm{NLI}}_k$ was received at time $t_{k'}$, the signal Σ at an arbitrary subsequent instant t_k will be updated according to

$$\Sigma_k \leftarrow \Sigma_{k'} + \langle \Delta\Sigma, \Delta\Sigma\rangle\ , \tag{10}$$

where the addition is carried out channel-wise, and the increment for each channel is

$$\Delta\Sigma = \left\lceil \frac{t_k - t_{k'}}{\tau_s \Delta k} \right\rceil . \tag{11}$$

Here, $\lceil\cdot\rceil$ denotes the ceiling function and Δk is an integer parameter defining the number of sampling periods that each channel will require to jump to the next integer.

If $\overline{\mathrm{NLI}}_k > 0$, there is no imminent risk of a voltage collapse, but resources may still be used as a preventive measure. The criterion for selecting Σ_{k+1} relies on the rate of change of $\overline{\mathrm{NLI}}_k$, since this indicator drops rapidly just before becoming negative [16]. The rate of change at time t_k is denoted by $\overline{\mathrm{NLI}}'_k$ and is computed as $\left(\overline{\mathrm{NLI}}_k - \overline{\mathrm{NLI}}_{k-1}\right)/\tau_s$. To discriminate slight from drastic changes, the second node in the decision tree compares $\overline{\mathrm{NLI}}'_k$ with an adjustable threshold $a < 0$.

If both conditions $\overline{\mathrm{NLI}}'_k > a$ and $\overline{\mathrm{NLI}}'_k = 0$ are met, a new stable equilibrium point may have been reached. Hence Σ_{k+1} preserves the current value Σ_k. If $\overline{\mathrm{NLI}}'_k > a$ but $\overline{\mathrm{NLI}}'_k \neq 0$, the signals $\langle 2,2\rangle$ and $\langle 3,3\rangle$ are selected depending on the

condition $\max(\widehat{\mathbf{I}}_F) < 1$, i.e. whether all the field currents are below their limit. Since $\overline{\text{NLI}}_k$ is not decreasing rapidly, the DERs and FLs need not be very responsive to these values.

Finally, if $\overline{\text{NLI}}_k^{'} \leq a$, more support is required. A second threshold $b < 0$ that satisfies $b < a$ is introduced to detect more severe situations. When $\overline{\text{NLI}}_k^{'}$ is bounded between b and a, and $\max(\widehat{\mathbf{I}}_F) < 1$, Σ_{k+1} is assigned the pair $\langle 3, 3\rangle$. Otherwise, it is assigned $\langle 4, 4\rangle$. It is when these values are issued that more DERs and possibly FLs should start to contribute.

Since the $\overline{\text{NLI}}$ usually takes values between 1.5 and -1, the rate of change $\overline{\text{NLI}}^{'}$ is bounded between $-2.5/\tau_s$ and $2.5/\tau_s$. Furthermore, since a and b should distinguish different values of $\overline{\text{NLI}}^{'}$, then $-2.5/\tau_s < b < a < 0$. One approach to set these parameters is to iterate over several pairs (a, b) that satisfy the previous inequalities, simulate expected disturbances, and select a pair that produces an appropriate dynamic response.

Once Σ_{k+1} has been selected, it is broadcast at time t_{k+1}, and the coordinator traverses the decision tree once again.

As an alternative to considering only one field current above the limit, a TSO may consider two or several field currents above the limits to request more participation from DERs and FLs. This will depend on the network characteristics and the number of machines in the system.

D. Steady-State Behavior and Restoration Process

After several tree traversals, the coordinator may reach the same leaf over and over again, indicating that a steady-state condition has been reached. However, it is possible for the coordinator to either over- or underestimate the support being required, thus leading to oscillations. To avoid this, a simple strategy to freeze the value of Σ is considered.

If the decision tree causes Σ to decrease at $t_{k'}$, the rate of change $\overline{\text{NLI}}_{k'}^{'}$ is recorded. When future values of $\overline{\text{NLI}}^{'}$ go below $\overline{\text{NLI}}_{k'}^{'}$, the support being requested is insufficient. In this case, the value found by traversing the tree is overridden and the signal is frozen at $\Sigma_{k'}$. Afterward, Σ can only change either because the tree asks for a larger value or because the TSO commands a restoration process. This command is issued when ν changes back from 1 to 0. If this change takes place at time $t_{k'}$, then Σ is updated at any later time t_k according to

$$\Sigma_k \leftarrow \Sigma_{k'} - \langle \Delta\Sigma, \Delta\Sigma\rangle \ , \tag{12}$$

where $\Delta\Sigma$ is the change given in (11) but possibly employing a different Δk. These increments cause Σ to decrease towards $\langle 1, 1\rangle$, the point at which all support is removed.

III. Local Control Actions

Each DER and FL has an independent controller that processes Σ and changes the unit's behavior based on local conditions. This paper considers inverter-interfaced DERs, Electric Water Heaters (EWHs), which represent Thermostatically Controlled Loads (TCLs), and Inverter-Interfaced Air Conditioners (IACs). Since the control strategies rely on internal timers and straight-forward calculations, the memory and processing requirements remain low. The clock inside each unit runs fast enough so that the changes in Σ are detected immediately.

A. Inverter-Interfaced DERs

Small-scale Photovoltaic (PV) systems and BESS are represented by the DER_D model, shown in Fig. 4. The details of this new model can be found in [34]. Contrary to other aggregate options such as the well-known PVD1 [42] or the DER_A [43], this model provides a more suitable representation of individual DERs installed at the LV level. It also imitates DER compliance with interconnection requirements of IEEE Std. 1547 [44].

The model presents two independent Proportional-Integral (PI) controllers to regulate the active and reactive power output. The reactive power control loop uses a volt-var curve to define the power setpoint Q_{ref} based on the voltage $\widehat{V}$ measured at the DER's terminals. The DER responds to the coordinator as long as $\widehat{V}$ lies between the volt-var parameters V_2 and V_3 [31]. For more severe network conditions, i.e. $\Sigma_Q \geq 3$, the value of V_2 (resp. V_3) may be reduced (resp. increased) to guarantee that the DER will remain within the coordinator's reach.

When the coordinator requests reactive power injections, the DER's reactive power setpoint changes by an amount

$$\Delta Q_{\text{ref}} = \rho \, \frac{V_3 - \widehat{V}}{V_3 - V_2} \, Q^{+}_{\text{DER}} \, , \tag{13}$$

where Q^{+}_{DER} is the maximum reactive power that the DER can inject at the time of request, and $0 \leq \rho \leq 0.3$ is used to regulate the responsiveness of the DER to avoid unnecessary overreactions [31]. After several coordinator requests, the DER may fully utilize its reactive power capacity; for details see [34]. For reactive power absorption, the setpoint changes by an amount

$$\Delta Q_{\text{ref}} = \rho \left(1 - \frac{V_3 - \widehat{V}}{V_3 - V_2} \right) Q^{-}_{\text{DER}} \, , \tag{14}$$

where Q^{-}_{DER} is the maximum reactive power that the DER can absorb. These setpoint changes are applied with a sampling period τ_{DER} that is a function of Σ_Q. When $\Sigma_Q = 1$, τ_{DER} is $5\,\text{s}$, and for $\Sigma_Q = 5$ it reduces to $1\,\text{s}$.

When the coordinator requests active power support, the DER changes its setpoint P^{*}_{DER} according to its possibilities. PV systems are only able to reduce their power injection (when $\Sigma_P < 0$), whereas BESSs can either reduce or increase their injection (when $\Sigma_P < 0$ or $\Sigma_P > 0$, respectively). This setpoint can take any value between P^{-}_{DER} and P^{+}_{DER}, the unit's thermal limits under the reactive power demand governed by (13) and (14). Since a reduction of active power generation would be counterproductive, this paper assumes $\Sigma_P > 0$, and hence the active-power setpoint of the PVs is left unchanged. Moreover, since the active power should be modified only in severe scenarios, the setpoint of any BESS is given the value halfway between its pre-disturbance power injection and P^{+}_{DER} when $\Sigma_P = 4$, and the value P^{+}_{DER} when $\Sigma_P = 5$.

B. Electric Water Heaters

The EWHs are represented by a zone-stratified thermal model that considers high-, mixed-, and low-temperature zones [45]. The hot water outlet is located at the high-temperature zone while the cold inlet is in the lower part.

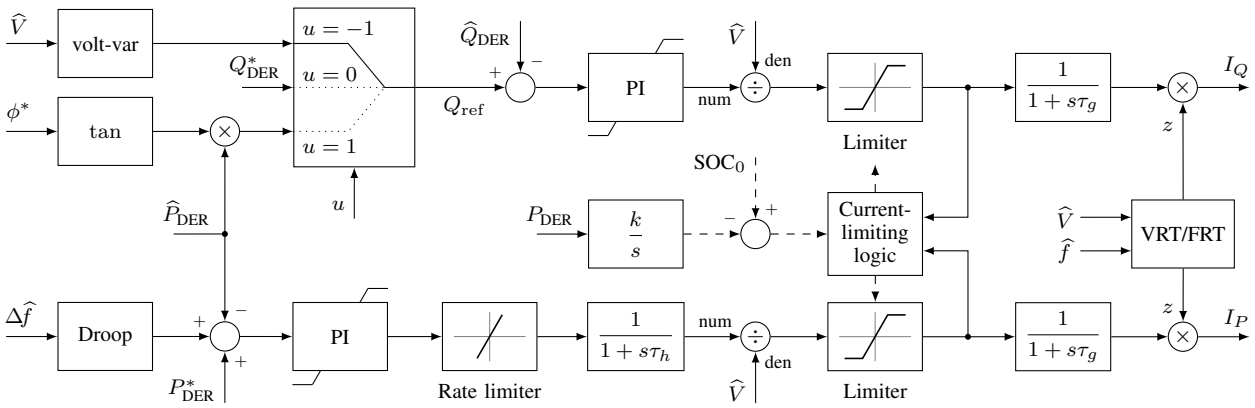

Fig. 4. Internal controls of the DER model. The circunflex, as in $\widehat{V}$ and $\widehat{f}$, denotes (possibly delayed) measurements, whereas the asterisk denotes setpoints.

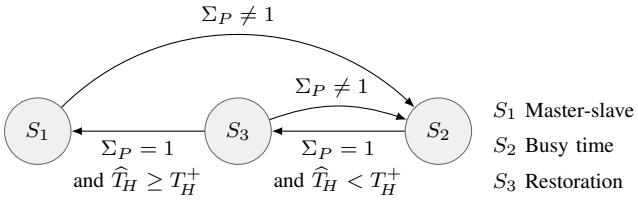

Fig. 5. Active-power control modes and associated transitions for EWHs.

The high-, mixed-, and low-temperatures are denoted by T_H, T_M, and T_L, respectively, and evolve according to the thermal model proposed in [45].

Two independent resistors are used to heat the water. When energized, they demand a power P_{WH} determined by the resistance and the applied voltage. The water temperature of the high and low zones are controlled by thermostats that follow a master-slave scheme. Here, only one of the heating elements is ON at a time. When both temperatures are outside their corresponding limits, the upper resistor is prioritized.

An EWH can respond to the coordinator requests by switching ON less frequently. For simplicity, it is assumed that the local controller acts on the bottom element alone. Certainly, the control of T_L is an indirect way of controlling T_H, since the former is a lower bound of the latter.

The control scheme is described by the Finite-State Machine (FSM) shown in Fig. 5. Under normal conditions with $\Sigma_P = 1$, the EWH operates autonomously, and follows the master-slave scheme (state S_1). It also records its duty cycle η and its period τ. Although the switching behavior is non-cyclic, η and τ can be approximated by measuring the state of the EWH over large time windows. It is then possible to define the busy time as $\tau_{\text{ON}} = \eta\tau$ and the idle time as $\tau_{\text{OFF}} = \tau - \tau_{\text{ON}}$, and use them to reduce the switching frequency.

Upon detecting a support request, i.e. $\Sigma_P \neq 1$, the EWH stops following the thermostats and starts behaving as a timed automaton to reduce the busy time (state S_2). An internal timer forces the unit to stay ON no longer than $\gamma\tau_{\text{ON}}$ and to stay OFF no longer than $\tau - \gamma\tau_{\text{ON}}$, where the constant $\gamma \leq 1$ is a decreasing function of Σ_P. Since the duty cycle of the unit is reduced, so is the aggregate demand of the EWH population.

When entering S_2, the participating EWH units do not switch OFF at the same time, as this would introduce artificial synchronization. Instead, for the units that were ON (resp. OFF) when entering state S_2, the local controller compares $\gamma\tau_{\text{ON}}$ (resp. $\tau - \gamma\tau_{\text{ON}}$) with the time that elapsed since the unit last switched ON (resp. switched OFF). This preserves the heterogeneity of the EWH population.

Once the coordinator stops requesting support, i.e. $\Sigma_P = 1$, the EWH enters the restoration process (state S_3). Because most temperatures could have exited the thermostat deadband during the event, returning to the master-slave scheme would, again, introduce synchronization. To prevent this, the local controller keeps behaving as a timed automaton, but now it increases the pre-disturbance busy time by a factor $\gamma' > 1$ that is large enough to bring T_H to its upper bound T_H^+. To ensure that the units with lower temperatures are restored faster, γ' depends on the value of T_L that was measured right before entering S_3, denoted $\widehat{T}_L^{\text{res}}$, and on the position of this measurement within a deadband of length ΔT_L and with upper bound T_L^+. This dependence is given by

$$\gamma' = \begin{cases} 1 + \Delta\gamma \left(\dfrac{T_L^+ - \widehat{T}_L^{\text{res}}}{\Delta T_L} \right) & \text{if } \widehat{T}_L^{\text{res}} \geq T_L^+ - \Delta T_L \,, \\ 1 + \Delta\gamma & \text{if } \widehat{T}_L^{\text{res}} < T_L^+ - \Delta T_L \,. \end{cases} \tag{15}$$

A value of $\Delta\gamma = 0.15$ and a deadband ΔT_L twice as large as the original thermostat deadband provide a good trade-off between the duration of the restoration process, and the overshoot in the aggregate demand.

C. Inverter-Interfaced Air Conditioners

Modern Air Conditioner (AC) units are equipped with inverters that modify the AC compressor frequency according to the temperature requirements. This control makes the AC unit operate continuously at a very low power demand.

A two-mass model is used to describe the room's thermal dynamics [46]. This thermal subsystem is coupled to the electrical subsystem as depicted in Fig. 6. The details of this model and its parameters can be found in [34]. The compressor frequency f_{AC} changes if the difference between the measured

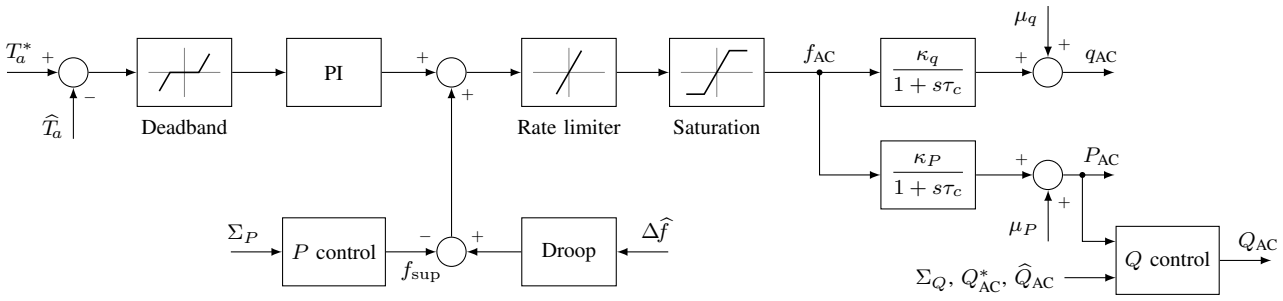

Fig. 6. Internal controls of an IAC.

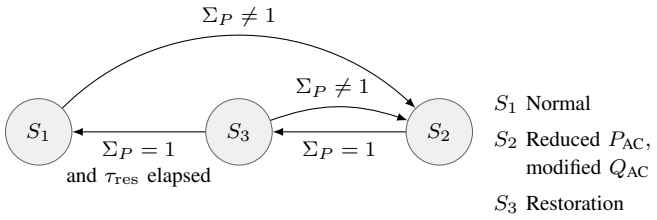

Fig. 7. Control modes and associated transitions for IACs.

air temperature $\widehat{T}_a$ and the desired temperature T_a^* is large enough to exceed the deadband. A PI controller is used to regulate this frequency. The active power demand P_{AC} and the heat extraction q_{AC} from the IAC unit are functions of f_{AC}; see [47] for details. Moreover, the reactive power demand Q_{AC} depends on the inverter's ability to demand or inject reactive power, according to the active power P_{AC} being demanded. It is assumed that the inverter can change its reactive power with a PI controller inside the Q-control block in Fig. 6.

The local control scheme is described by the FSM shown in Fig. 7. Under normal conditions (state S_1), the IAC operates at a frequency f_{AC} that keeps $\widehat{T}_a$ within the deadband.

After detecting $\Sigma_P \neq 1$, the IAC modifies either its active or its reactive power demand depending on the level of support being requested (state S_2). For moderate levels, the setpoint of reactive power demand is changed to

$$Q^*_{\text{AC}} = -\gamma_Q \sqrt{S_{\text{n}}^2 - P_{\text{AC}}^2}\,, \tag{16}$$

where S_{n} is the nominal power of the IAC and the parameter $\gamma_Q \leq 1$ is an increasing function of Σ_Q. For higher levels of support, when the reactive power has been exhausted, the active power is allowed to change by increasing f_{sup} to the value

$$f_{\text{sup}} = \gamma_P (f_{\text{AC}} - f^-_{\text{AC}})\,, \tag{17}$$

where $\gamma_P \leq 1$ is an increasing function of Σ_P, whereas f^-_{AC} is the lower bound of the saturation block in Fig. 6. Since f_{sup} is subtracted from the output of the PI controller, setting $\gamma_P = 0$ would leave f_{AC} unchanged, while setting $\gamma_P = 1$ would cause f_{AC} to hit its lower bound.

When the coordinator stops requesting support, the IAC enters a restoration process (state S_3). Although the effects of a synchronized restoration would not be as harmful as in the case of the EWHs, it is still convenient that the IACs restore to normal conditions smoothly rather than abruptly. To this end, f_{AC} is restored linearly in time during a period τ_{res}.

The actions of DERs and FLs to support the TN in emergency conditions are not expected to violate constraints in the DN. In terms of voltages, the active power demand reduction of FLs and the reactive power injection of DERs will help to improve the local voltages. Moreover, the local controllers could be adapted to cease participation if an overvoltage condition was encountered. In terms of potential overloadings, the power demand reduction of FLs should compensate for the reactive power injections of DERs. If not, any overloading condition due to reverse reactive currents will be mild and temporary, which can be withstood by transformers and cables. A more sophisticated scheme to avoid overloadings will require more measurements and communication infrastructure to request a group of DERs to cease participation during the detected overloading condition. This, however, will reduce the availability of DERs, and thus the capacity of the coordinator to provide support to the TN.

IV. Simulation Results

The coordination scheme was validated through dynamic T-D co-simulations, as they capture the interaction between the TN and the LV networks. To test the performance with and without the coordinator, the system was subjected to two disturbances of different severity. Both cases were simulated with RAMSES, a time-domain power system simulator [48].

A. Simulation Setup

The T-D test system has more than 4000 buses and is depicted in Fig. 8. The TN model is based on the four-bus system introduced in [8] to study long-term voltage instability. Most of the power is supplied from bus 1 by a remote, stiff system, modeled by a Thévenin equivalent. The rest is supplied by a large synchronous generator g_2 at bus 2 that is equipped with a first-order Automatic Voltage Regulator (AVR). Buses 1 and 4 are connected by a double-circuit transmission corridor, whose length was increased to favor voltage instability conditions. The load at bus 3, which amounts to 20 MW and 10 Mvar at nominal voltage, is fed through a transformer with an OLTC.

Due to computational constraints, one fraction of the load was modeled using aggregate elements whereas the other was modeled explicitly. The aggregate elements are an induction

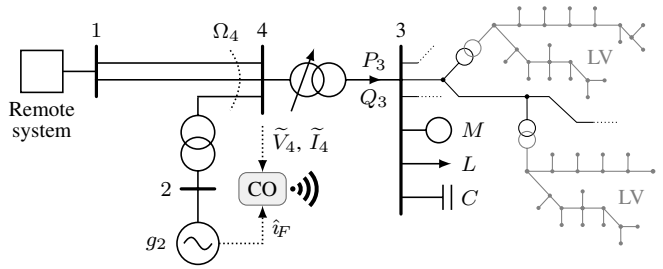

Fig. 8. Test system with explicit modeling of HV, MV, and LV networks. The coordinator (CO) sends signals to DERs and FLs.

TABLE I
DER AND FL CONTROL PARAMETERS AS FUNCTIONS OF Σ.

	DERs		EWHs	IACs	
Σ	ρ	τ_{DER} (s)	γ	γ_P	γ_Q
$\langle 1,1\rangle$	0	5	1	0	0
$\langle 2,2\rangle$	0.15	1	1	0	0.25
$\langle 3,3\rangle$	0.3	1	0.8	0	0.75
$\langle 4,4\rangle$	0.3	1	0.6	0.5	1
$\langle 5,5\rangle$	0.3	1	0.1	1	1

motor M that demands $10\,\text{MW}$ with a power factor of 0.84 lagging, a voltage-sensitive load L that demands $5\,\text{MW}$ at nominal voltage with a power factor of 0.94 lagging, and a fixed-step shunt capacitor bank C that injects $4\,\text{Mvar}$ at nominal voltage. The induction motor is an aggregate representation of many similar industrial motors fed by the same substation. It was included to consider fast restoring loads and high reactive power demands during low voltage conditions. Since this is an aggregate representation, a third-order model with constant mechanical torque was used. All static loads were modeled as exponential loads [8] with exponents of 1.5 and 2.5 for active and reactive power, respectively.

The individual elements that were modeled explicitly are spread over several LV networks [49] connected to the same MV feeder [50], which comprise over 4200 buses integrated along with the TN model using the methodology from [51]. These LV networks host 284 PV systems, 526 BESSs in charging and 39 in discharging state, 590 IACs, and 1164 EWHs. Although the proposed coordination could also manage larger DERs and FLs connected to the MV network, this paper focuses on coordinating small-scale units at the LV level. The initial conditions are such that the EWH population is heterogeneous, i.e. non-synchronized, and the reactive power output of the PV systems and BESSs lies on the volt-var curve.

The coordinator receives PMU measurements of the phasor voltage $\widetilde{V}_4$ at bus 4 and the phasor currents entering Ω_4 to obtain $\widetilde{I}_4$, and uses them to compute $\overline{\text{NLI}}$ and $\overline{\text{NLI}}'$. In this test case, $\overline{\text{NLI}}$ is computed using $M = 350$, $M_d = 10$, and $\varepsilon = 0.001$. The coordinator also receives the normalized field current $\hat{\imath}_F$ of g_2 and the binary signal ν. A sampling period $\tau_s = 1\,\text{s}$ and a signal with $\Sigma_P = \Sigma_Q$ are assumed in order to illustrate the effectiveness of a coordination scheme with low communication requirements. The thresholds of the decision tree were set to $a = -0.02$ and $b = -0.1833$. Additionally, Σ is increased (resp. reduced) every $\Delta k = 5$ sampling periods when $\overline{\text{NLI}} < 0$ (resp. $\nu = 0$).

The local controllers of the DERs and FLs use the parameters reported in Table I. It can be seen that ρ, τ_{DER}, and γ_Q tend to exhaust the reactive power before the active power, associated to γ and γ_P. Finally, the restoration periods τ_{res} of the IACs are uniformly distributed between $5\,\text{min}$ and $10\,\text{min}$.

B. Response to Three-Phase Fault

In the first scenario, a six-cycle short-circuit takes place halfway between buses 1 and 4 at $t = 10\,\text{s}$, which causes one of the circuits to trip. This shrinks the capacity of the transmission system to supply power to the load at bus 3, while the latter is being restored by the OLTC actions. This is a typical mechanism of long-term voltage instability driven by the restoration of voltage-dependent loads [8].

Without the coordinator (dotted curves in Figs. 9a to 9d), the voltage reduction that follows the fault (Fig. 9a) is only counteracted by the OLTC, the AVR of g_2, and, to a lesser extent, the volt-var control of the DERs. However, given that the AVR raises $\hat{\imath}_F$ above 1 (Fig. 9b), i.e. above the thermal limit of the field winding, the support cannot be sustained and is withdrawn after $1\,\text{min}$ and $23\,\text{s}$ by the OEL. While the active power P_4 entering bus 4 remains practically constant (Fig. 9c) due to the reduced power-transfer limit of the TN, the conductance G_4 increases with each action of the OLTC. Although the $\overline{\text{NLI}}$ does point to an emergency after $1\,\text{min}$ and $30\,\text{s}$ (Fig. 9d), the lack of remedial actions leads to a voltage collapse (the undervoltage protections of g_2 were not modeled).

With the coordinator (solid curves in Fig. 9), support is requested by increasing Σ (superimposed on Figs. 9e to 9i) as soon as the first $\overline{\text{NLI}}$ values are obtained at about $30\,\text{s}$. It is assumed that the circuit tripping was detected immediately, and thus $\nu = 1$. Because $\overline{\text{NLI}}' > a$ and $\hat{\imath}_F > 1$, the tree traversal terminates in $\langle 3,3\rangle$, and this makes up the first request.

The most immediate contributions are made by the units capable of generating reactive power. The output of the DERs (Fig. 9e) is nonzero for some units before the fault, due to the local volt-var control, and then for all units after the undervoltage is detected. Once Σ_Q is no longer 1, the units start following the coordinator as long as their terminal voltage $\widehat{V}$ lies between the volt-var parameters $V_2 = 0.975\,\text{pu}$ and $V_3 = 1.025\,\text{pu}$. Their final power output is governed by the current-limiting logic, which depends on the unit's nominal power. The output of the IACs (Fig. 9f), which are devoid of any local voltage control, maintains its initial value even during the first undervoltage. However, the reactive power output also changes when requested by the coordinator, which leads to a power-flow reversal.

The reactive power support suffices to stabilize P_4 and G_4 during the first two minutes. Furthermore, it prevents $\hat{\imath}_F$ from increasing with each OLTC action and hence it delays until $t = 2\,\text{min}$ the action of the OEL, which has an inverse-time characteristic. If no further support were provided, the transmission voltages would probably collapse later, as suggested by the sudden voltage drop that follows the OEL action. It must be noted that right after $\hat{\imath}_F$ is brought below 1, the tree traversal terminates in $\langle 2,2\rangle$, since $\overline{\text{NLI}}' \neq 0$. The

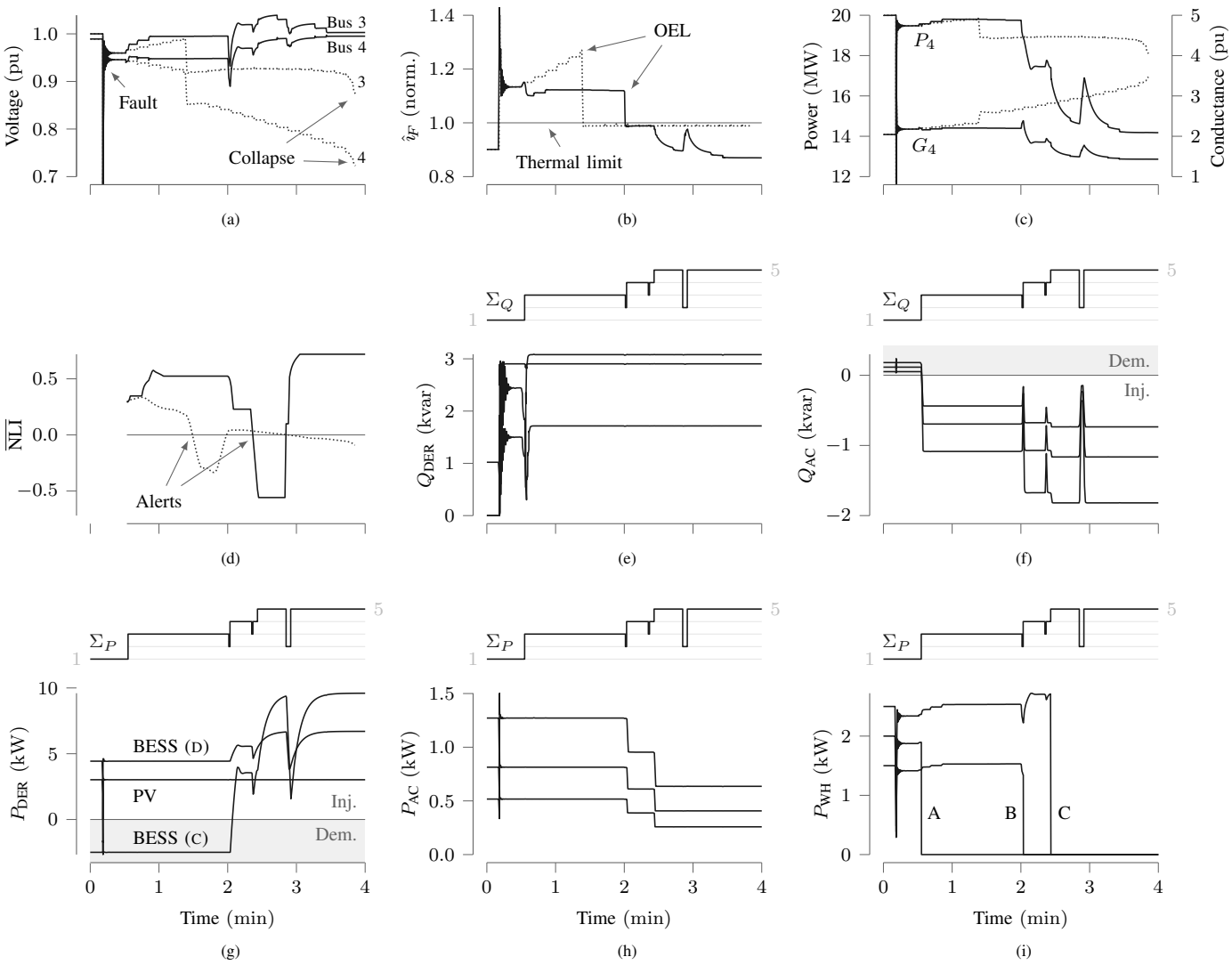

Fig. 9. Response to three-phase fault and the subsequent circuit tripping. All plots share the horizontal axis (time) and some of them were cropped vertically to exclude fast, unimportant transients. In plots (a) to (d), the solid curves show the response with a coordinator and the dotted curves show the response without it. In plots (e) to (i), the relevant channel Σ_P or Σ_Q (both take the same values) is shown above the response of individual DERs and FLs chosen arbitrarily.

coordinator thus attempts to request less support at $t = 2\,\text{min}$ given the apparent favorable conditions, but this attempt is unsuccessful. The $\overline{\text{NLI}}$ drops immediately afterwards and hence Σ is raised to $\langle 4, 4\rangle$ and even to $\langle 5, 5\rangle$. This is the maximum level of support that can be requested and requires the active power reserves to be exhausted as well.

The active power contribution of the DERs depends on their capabilities, as depicted in Fig. 9g both for PV systems and BESSs. The PV systems maintain their active power generation nearly constant, given that they are assumed to perform Maximum Power Point Tracking (MPPT). The BESSs that were in discharging state (D) increase their injection until hitting the limit imposed by the current-limiting logic. Finally, the BESSs that were in charging state (C) undergo a power-flow reversal and start injecting power instead of demanding it.

The active power contribution of the IACs becomes noticeable as soon as $\Sigma = \langle 4, 4\rangle$, and even more for $\Sigma = \langle 5, 5\rangle$; see Fig. 9h. Because γ_P takes the values 0.5 and 1 for these levels of request, respectively, the active power demand of the IACs is first reduced halfway towards the minimum power allowed by the unit's compressor, and then to that value. This reduction makes room for additional reactive power, and causes it to increase immediately without exceeding the unit's rating.

Although the aggregate demand of the EWH population is roughly proportional to γ, the individual contributions can only be analyzed by considering the past behavior of each unit, as shown in Fig. 9i. Given that $\gamma = 0.8$ for $\Sigma = \langle 3, 3\rangle$, only a minority of the units that are ON when receiving this value of Σ should switch OFF (in fact, only about 20% of the EWH population). One such example is unit A, which had completed more than 80% of its average switching period when requested to contribute. Other units, such as B and C, find themselves in an earlier position of their period, and hence switch OFF only for higher values of Σ. It is important to recall that this position is taken into account by the local timers to preserve heterogeneity.

All these cumulative efforts cause a significant reduction in both P_4 and $\hat{\imath}_F$, and thus prevent a voltage collapse. Shortly

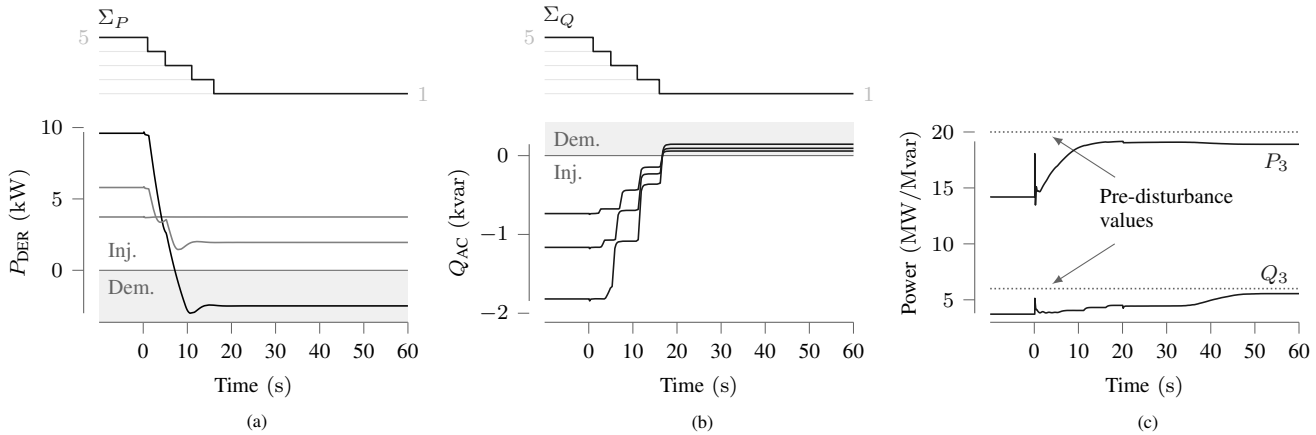

Fig. 10. Restoration process. Plots (a) and (b) show the active power of individual DERs and the reactive power of individual IACs, respectively. Plot (c) shows the active and reactive power demanded at bus 3. These plots are a continuation of Fig. 9 after the system reached a new steady state. The restoration begins at $t = 0\,\text{s}$.

before the third minute, the coordinator makes yet another attempt to reduce Σ, caused by a steep increase of $\overline{\text{NLI}}$ that suggests favorable conditions. However, after $\overline{\text{NLI}}$ comes to a standstill, the coordinator detects that $\overline{\text{NLI}}'$ decreases and hence it freezes Σ at $\langle 5, 5\rangle$. Since $\hat{\imath}_F < 1$, the system reaches a new steady state that can be maintained for several minutes until other remedial actions, not involving demand resources, are used by the TSO.

Once the tripped circuit is brought back into operation, then $\nu = 0$, and the coordinator reduces Σ gradually towards $\langle 1, 1\rangle$. Figures 10a and 10b show the restoration of the active power of DERs and the reactive power of IACs. Given the choice of Δk, this process is completed in $20\,\text{s}$. For the active power of the IACs and the EWHs, the restoration takes place in a time frame of several minutes, as this avoids an undesired synchronization.

As shown in Fig. 10c, the power delivered by the step-down transformer to bus 3, denoted by P_3 and Q_3 in Fig. 8, does not return exactly to the pre-disturbance values due to the new demand of the voltage-dependent loads, and because not all the FLs have been fully restored at the end of this simulation.

C. Response to Three-Phase Fault Followed by Reduction of Shunt Compensation

In the second scenario, the short-circuit is followed by a $1\,\text{Mvar}$ reduction of the shunt compensation provided by C after about $2\,\text{min}$ and $45\,\text{s}$. Albeit unlikely, this condition tests the coordinator under narrower reactive power margins.

Without the coordinator, the additional disturbance accelerates the voltage collapse so that it takes place shortly before the third minute, as shown in Fig. 11a. With the coordinator, instead, the compensation loss is not critical, since the reactive power margin of g_2 has been enlarged through the actions of the DERs and IACs. The fact that these units made contributions can be recognized in the evolution of the $\overline{\text{NLI}}$ presented in Fig. 11b, which evolves similar to how it did in the previous scenario, and in the evolution of the total power supplied to the load, shown in Fig. 11c.

The participation of thousands of small-scale units to support TNs in emergency conditions still requires more research and testing before its implementation. The adjustments of devices to receive and process the signals in a framework of Internet of Things (IoT), the possible user's discomfort, and the economic compensations were not covered in this piece of research, but need to be examined in the coming years, as the decentralization of generation gains ground in modern power systems.

D. Coordination with a Load Shedding Scheme

In the last scenario, the coordinator operates jointly with selective load shedding (CO + LS). Besides steering the DERs and FLs, the signal Σ is used to trip certain MV feeders from the explicitly-modeled DN. About half of these feeders are tripped when $\Sigma = \langle 3, 3\rangle$, and the rest is tripped when $\Sigma = \langle 4, 4\rangle$, leading to a total load loss of $5\,\text{MW}$. For comparison, a simulation with LS alone is presented. The same disturbance and initial conditions from Section IV-B were used for both simulations.

Figure 12 shows the voltage and power demands at bus 3 after the short-circuit and the subsequent line tripping. With CO + LS, only the first stage of LS was used as Σ stayed in $\langle 3, 3\rangle$. While some agents get isolated with the feeder disconnection at $t = 34\,\text{s}$, the other DERs and FLs remain online and modify their power to an extent that makes further LS unnecessary. Their contribution brings $\hat{\imath}_F$ to 0.98 with no OEL activation. With LS alone, the second stage was used when $\Sigma = \langle 4, 4\rangle$ at $t = 49\,\text{s}$, which restores V_3 above the OLTC deadband, and lowers $\hat{\imath}_F$ to 0.93.

As shown in these simulations, the proposed coordinator operates as a new line of defense against voltage instability conditions. Moreover, the participation of DERs and FLs reduces the amount of load to be shed when compared to LS alone.

V. Conclusion

The challenge of providing services to TNs from thousands of small-scale units located at LV poses high complexity given the low level of observability and the large number of units to be coordinated. To favor the principles of applicability, scalability, and low computational demands, the proposed coordinator

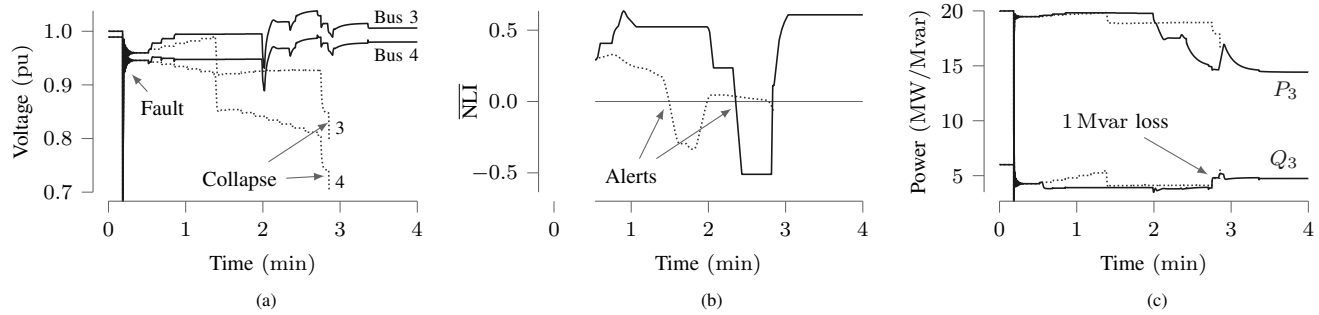

Fig. 11. Response to three-phase fault, circuit tripping, and 1 Mvar loss. Plot (a) shows the voltage evolution at buses 3 and 4, plot (b) shows the $\overline{\text{NLI}}$ measured at bus 4, and plot (c) shows the active and reactive power demanded at bus 3. The responses with a coordinator (solid lines) and without it (dotted lines) are shown.

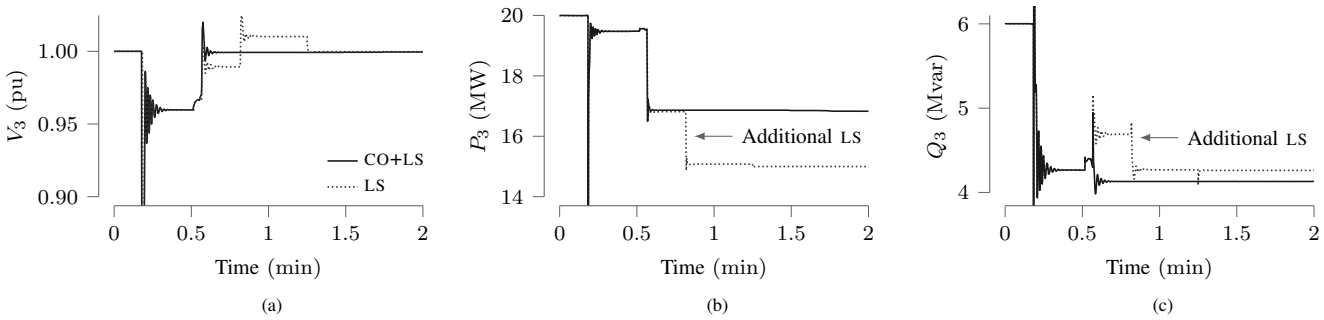

Fig. 12. System response for coordinator in combination with load shedding (CO + LS, solid lines), and load shedding alone (LS, dotted lines). Plot (a) shows the voltage evolution at bus 3. Plots (b) and (c) show the active and reactive power demanded at bus 3, respectively.

deviates significantly from the concept of a central entity with full knowledge of the network and its active components.

This new model-free coordinator sends signals to the downstream devices only when participation is needed, but receives null information from their actual conditions. The DERs and FLs have autonomy in the sense that they choose when and how to participate based on the received signals and their local conditions, e.g. the terminal voltage regulated by the volt-var control of PVs, the room temperatures controlled by IACs, and the water temperatures controlled by EWHs.

The simulation results, with explicit models of HV, MV, and LV networks, suggest that it will be possible to support the bulk TN with the contribution of hundreds or thousands of small-scale units that do not know the overall system performance, but can surely contribute to save a power system from a blackout. The signals allow the coordinator to request support to DERs and FLs according to the severity of the disturbance being faced. Hence, the coordinator can steer the devices to reach the desired target without overshooting or exhausting the demand resources. This coordinator is not expected to operate alone, but jointly with more classical countermeasures against voltage instability conditions, given that the actual contribution of DERs and FLs will depend on their availability and penetration levels.

Future research efforts will focus on providing new features to the coordinator so that it can predict future system conditions, and anticipate the control actions accordingly. Moreover, future work will look at the coordination between multiple substations, not considered in this paper, which could potentially lead to a more efficient use of the available resources. Also, the quantification of the required active and reactive power exchange at the TN-DN interconnections will be key to avoid excessive participation of DERs and FLs. To this extent, larger test systems with multiple substations and independent coordinators will be used.

REFERENCES

[1] D. Mayorga Gonzalez, J. Myrzik, and C. Rehtanz, "The smart power cell concept: Mastering TSO-DSO interactions for the secure and efficient operation of future power systems," *IET Generation, Transmission & Distribution*, vol. 14, no. 13, pp. 2407–2418, May 2020.

[2] H. Sun, Q. Guo, J. Qi, V. Ajjarapu, R. Bravo, J. Chow, Z. Li, R. Moghe, E. Nasr-Azadani, U. Tamrakar *et al.*, "Review of challenges and research opportunities for voltage control in smart grids," *IEEE Trans. Power Syst.*, vol. 34, no. 4, pp. 2790–2801, Jul. 2019.

[3] A. G. Givisiez, K. Petrou, and L. F. Ochoa, "A review on TSO-DSO coordination models and solution techniques," *Electric Power Systems Research*, vol. 189, p. 106659, Aug. 2020.

[4] S. Bernard, G. Trudel, and G. Scott, "A 735 kV shunt reactors automatic switching system for Hydro-Québec network," *IEEE Trans. Power Syst.*, vol. 11, no. 4, pp. 2024–2030, Nov. 1996.

[5] T. Van Cutsem, "Voltage instability: Phenomena, countermeasures, and analysis methods," *Proc. IEEE*, vol. 88, no. 2, pp. 208–227, Feb. 2000.

[6] F. Capitanescu, B. Otomega, H. Lefebvre, V. Sermanson, and T. Van Cutsem, "Decentralized tap changer blocking and load shedding against voltage instability: Prospective tests on the RTE system," *International Journal of Electrical Power & Energy Systems*, vol. 31, no. 9, pp. 570–576, Mar. 2009.

[7] P. Aristidou, G. Valverde, and T. Van Cutsem, "Contribution of distribution network control to voltage stability: A case study," *IEEE Trans. Smart Grid*, vol. 8, no. 1, pp. 106–116, Jan. 2017.

[8] T. Van Cutsem and C. Vournas, *Voltage stability of electric power systems*. Springer Science & Business Media, 1998.

[9] B. Otomega and T. Van Cutsem, "Undervoltage load shedding using distributed controllers," *IEEE Trans. Power Syst.*, vol. 22, no. 4, pp. 1898–1907, Nov. 2007.

[10] G. Valverde and T. Van Cutsem, "Control of dispersed generation to regulate distribution and support transmission voltages," in *IEEE Grenoble Conf.*, Jun. 2013, pp. 1–6.

[11] D. B. Arnold, M. D. Sankur, M. Negrete-Pincetic, and D. S. Callaway, "Model-free optimal coordination of distributed energy resources for provisioning transmission-level services," *IEEE Trans. Power Syst.*, vol. 33, no. 1, pp. 817–828, Jan. 2018.

[12] E. Namor, F. Sossan, R. Cherkaoui, and M. Paolone, "Control of battery storage systems for the simultaneous provision of multiple services," *IEEE Trans. Smart Grid*, vol. 10, no. 3, pp. 2799–2808, May 2019.

[13] G. Coletta, A. Laso, G. M. Jónsdóttir, M. Manana, D. Villacci, A. Vaccaro, and F. Milano, "On-line control of DERs to enhance the dynamic thermal rating of transmission lines," *IEEE Trans. Sustain. Energy*, vol. 11, no. 4, pp. 2836–2844, Oct. 2020.

[14] G. Prionistis, T. Souxes, and C. Vournas, "Voltage stability support offered by active distribution networks," *Electric Power Systems Research*, vol. 190, p. 106728, Aug. 2021.

[15] L. Robitzky, D. Mayorga Gonzalez, C. Kittl, C. Strunck, J. Zwartscholten, S. Muller, U. Hager, J. Myrzik, and C. Rehtanz, "Impact of active distribution networks on voltage stability of electric power systems," in *IREP Bulk Power Systems Dynamics and Control Symposium*, Aug. 2017, pp. 1–10.

[16] C. D. Vournas, C. Lambrou, and P. Mandoulidis, "Voltage stability monitoring from a transmission bus PMU," *IEEE Trans. Power Syst.*, vol. 32, no. 4, pp. 3266–3274, Jul. 2017.

[17] L. Robitzky, U. Häger, and C. Rehtanz, "Modelling of active distribution networks and its impact on the performance of emergency controls," in *Power Systems Computation Conference*. IEEE, Jun. 2018, pp. 1–7.

[18] L. D. Pabón Ospina and T. Van Cutsem, "Power factor improvement by active distribution networks during voltage emergency situations," *Electric Power Systems Research*, vol. 189, p. 106771, Dec. 2020.

[19] F. Capitanescu, "TSO-DSO interaction: Active distribution network power chart for TSO ancillary services provision," *Electric Power Systems Research*, vol. 163, pp. 226–230, Jul. 2018.

[20] J. Silva, J. Sumaili, R. J. Bessa, L. Seca, M. A. Matos, V. Miranda, M. Caujolle, B. Goncer, and M. Sebastian-Viana, "Estimating the active and reactive power flexibility area at the TSO-DSO interface," *IEEE Trans. Power Syst.*, vol. 33, no. 5, pp. 4741–4750, Sep. 2018.

[21] S. Stanković and L. Söder, "Probabilistic reactive power capability charts at DSO/TSO interface," *IEEE Trans. Smart Grid*, vol. 11, no. 5, pp. 3860–3870, Sep. 2020.

[22] D. A. Contreras and K. Rudion, "Impact of grid topology and tap position changes on the flexibility provision from distribution grids," in *IEEE PES Innovative Smart Grid Technologies Europe*, 2019, pp. 1–5.

[23] S. Stanković, L. Söder, Z. Hagemann, and C. Rehtanz, "Reactive power support adequacy at the DSO/TSO interface," *Electric Power Systems Research*, vol. 190, p. 106661, Aug. 2021.

[24] P. Cicilio, E. Cotilla-Sanchez, B. Vaagensmith, and J. P. Gentle, "Transmission hosting capacity of distributed energy resources," *IEEE Trans. Sustain. Energy*, vol. 12, no. 2, pp. 794–801, Apr. 2021.

[25] Z. Li, Q. Guo, H. Sun, J. Wang, Y. Xu, and M. Fan, "A distributed transmission-distribution-coupled static voltage stability assessment method considering distributed generation," *IEEE Trans. Power Syst.*, vol. 33, no. 3, pp. 2621–2632, May 2018.

[26] L. D. Pabón Ospina and T. Van Cutsem, "Emergency support of transmission voltages by active distribution networks: A non-intrusive scheme," *IEEE Trans. Power Syst.*, 2020.

[27] A. Oulis-Rousis, D. Tzelepis, Y. Pipelzadeh, G. Strbac, C. D. Booth, and T. Green, "Provision of voltage ancillary services through enhanced TSO-DSO interaction and aggregated distributed energy resources," *IEEE Trans. Sustain. Energy*, vol. 12, no. 2, Apr. 2021.

[28] M. Obi, T. Slay, and R. Bass, "Distributed energy resource aggregation using customer-owned equipment: A review of literature and standards," *Energy Reports*, vol. 6, pp. 2358–2369, Sep. 2020.

[29] L. Gutierrez-Lagos, K. Petrou, and L. F. Ochoa, "Quantifying the effects of medium voltage-low voltage distribution network constraints and distributed energy resource reactive power capabilities on aggregators," *IET Generation, Transmission & Distribution*, pp. 1–14, Feb. 2021.

[30] V. Rigoni, D. Flynn, and A. Keane, "Coordinating demand response aggregation with LV network operational constraints," *IEEE Trans. Power Syst.*, vol. 36, no. 2, pp. 979–990, Mar. 2021.

[31] G. Valverde, D. Shchetinin, and G. Hug-Glanzmann, "Coordination of distributed reactive power sources for voltage support of transmission networks," *IEEE Trans. Sustain. Energy*, vol. 10, no. 3, pp. 1544–1553, Jul. 2019.

[32] S. Karagiannopoulos, C. Mylonas, P. Aristidou, and G. Hug, "Active distribution grids providing voltage support: The Swiss case," *IEEE Trans. Sustain. Energy*, vol. 12, no. 1, pp. 268–278, Jan. 2020.

[33] S. Karagiannopoulos, J. Gallmann, M. González Vayá, P. Aristidou, and G. Hug, "Active distribution grids offering ancillary services in islanded and grid-connected mode," *IEEE Trans. Smart Grid*, vol. 11, no. 1, pp. 623–633, Jan. 2020.

[34] J. García, J. Víquez, J. Incer, F. Escobar, P. Aristidou, and G. Valverde, "Modeling framework and coordination of DER and flexible loads for ancillary service provision," in *Proc. of the 54th Hawaii Int. Conf. on System Sciences*, Jan. 2021, p. 3111.

[35] C. Vournas, C. Lambrou, I. Anagnostopoulos, G. Christoforidis, and J. Kabouris, "Distributed reactive support and voltage stability limits: The example of Peloponnese in the Hellenic Interconnected System," in *Proc. of 2015 IEEE Power & Energy Soc. General Meet.*, Jul. 2015, pp. 1–5.

[36] D. Mayorga Gonzalez, J. Hachenberger, J. Hinker, F. Rewald, U. Häger, C. Rehtanz, and J. Myrzik, "Determination of the time-dependent flexibility of active distribution networks to control their TSO-DSO interconnection power flow," in *Power Systems Computation Conference*. IEEE, 2018, pp. 1–8.

[37] N. Hatziargyriou, J. V. Milanovic, C. Rahmann, V. Ajjarapu, C. Canizares, I. Erlich, D. Hill, I. Hiskens, I. Kamwa, B. Pal, P. Pourbeik, J. J. Sanchez-Gasca, A. M. Stankovic, T. Van Cutsem, V. Vittal, and C. Vournas, "Definition and classification of power system stability — Revisited & extended," *IEEE Trans. Power Syst.*, Dec. 2020.

[38] M. Glavic and T. Van Cutsem, "Wide-area detection of voltage instability from synchronized phasor measurements. Part I: Principle," *IEEE Trans. Power Syst.*, vol. 24, no. 3, pp. 1408–1416, Aug. 2009.

[39] S. Dasgupta, M. Paramasivam, U. Vaidya, and V. Ajjarapu, "Real-time monitoring of short-term voltage stability using PMU data," *IEEE Trans. Power Syst.*, vol. 28, no. 4, pp. 3702–3711, Nov. 2013.

[40] C. D. Vournas and T. Van Cutsem, "Local identification of voltage emergency situations," *IEEE Trans. Power Syst.*, vol. 23, no. 3, pp. 1239–1248, Aug. 2008.

[41] C. Lambrou, P. Mandoulidis, and C. Vournas, "Validation of voltage instability detection and control using a real power system incident," *Energies*, vol. 14, no. 21, p. 7165, Nov. 2021.

[42] R. Elliott, A. Ellis, P. Pourbeik, J. Sanchez-Gasca, J. Senthil, and J. Weber, "Generic photovoltaic system models for WECC — A status report," in *Proc. of 2015 IEEE Power & Energy Soc. General Meet.*, 2015, pp. 1–5.

[43] "Reliability guideline: Parametrization of the DER_A model," NERC, Atlanta, Tech. Rep., Sep. 2019.

[44] "IEEE standard for interconnection and interoperability of distributed energy resources with associated electric power systems interfaces," *IEEE Std. 1547-2018 (Revision of IEEE Std. 1547-2003)*, pp. 1–138, Apr. 2018.

[45] M. Zuñiga, K. Agbossou, A. Cardenas, and L. Boulon, "Parameter estimation of electric water heater models using extended Kalman filter," in *Proc. of the 43rd Annual Conf. of the IEEE Ind. Electron. Soc., Beijing*, Oct. 2017, pp. 386–391.

[46] W. Zhang, J. Lian, C.-Y. Chang, and K. Kalsi, "Aggregated modeling and control of air conditioning loads for demand response," *IEEE Trans. Power Syst.*, vol. 28, no. 4, pp. 4655–4664, Nov. 2013.

[47] H. Hui, Y. Ding, and M. Zheng, "Equivalent modeling of inverter air conditioners for providing frequency regulation service," *IEEE Trans. Ind. Electron.*, vol. 66, no. 2, pp. 1413–1423, Feb. 2019.

[48] P. Aristidou, S. Lebeau, and T. Van Cutsem, "Power system dynamic simulations using a parallel two-level Schur-complement decomposition," *IEEE Trans. Power Syst.*, vol. 31, no. 5, pp. 3984–3995, 2015.

[49] C. Fennan, "Creation of a generic test case for combined simulations of medium and low voltage networks," ETH Zürich, Semester thesis, 2018.

[50] Distributed Generation and Sustainable Electrical Energy Centre. (2015) United Kingdom Generic Distribution System (UK GDS). [Online]. Available: https://github.com/sedg/ukgds

[51] F. Escobar, J. García, J. M. Víquez, G. Valverde, and P. Aristidou, "A combined high-, medium-, and low-voltage test system for stability studies with DERs," *Electric Power Systems Research*, vol. 189, p. 106671, Dec. 2020.